

Tunneling and mode conversion of fast magnetosonic waves in the magnetospheres of Earth and Mercury

YEVGEN O. KAZAKOV¹† AND TÜNDE FÜLÖP²

¹Laboratory for Plasma Physics, Royal Military Academy, LPP-ERM/KMS, TEC Partner, Brussels, BE-1000, Belgium

²Department of Applied Physics, Chalmers University of Technology, Göteborg, SE-41296, Sweden

(Received ?; revised ?; accepted ?. - To be entered by editorial office)

Narrow-band linearly polarized waves, having a resonant structure and a peak frequency between the local cyclotron frequency of protons and heavy ions, have been detected in the magnetospheres of Earth and of Mercury. Some of these wave events have been suggested to be driven by linear mode conversion (MC) of the fast magnetosonic waves at the ion-ion hybrid (IIH) resonances. Since the resonant IIH frequency is linked to the plasma composition, solving the inverse problem allows one to infer the concentration of the heavy ions from the measured frequency spectra. In this paper, we identify the conditions when the MC efficiency is maximized in the magnetospheric plasmas and discuss how this can be applied for estimating the heavy ion concentration in the magnetospheres of Earth and Mercury.

PACS codes:

1. Introduction

Heavy ion species are typically present in the magnetospheric plasmas surrounding the planets. The origin of heavy ions can be quite different depending on the planetary environment. For example, a significant fraction of He^+ and O^+ ions, originating from the polar wind and the outflow of ionospheric ions is present in some regions of the terrestrial magnetosphere ([André and Yau 1997](#); [Yau and André 1997](#)). The magnetosphere of Mercury is known to have a powerful exospheric source of Na^+ ions due to the sputtering of the planet's surface and subsequent photoionization. [Ip \(1986\)](#) estimated the content of the sodium ions to be $\geq 10\%$, and [Cheng et al. \(1987\)](#) concluded that the sodium ion source is at least comparable to, or can be greater than the solar wind source of protons. Recent MESSENGER measurements also confirmed that in some regions near Mercury, especially the nightside equatorial region, the Na^+ pressure can be a substantial fraction of the proton pressure ([Zurbuchen et al. 2011](#)). Another interesting example of the heavy ion abundance is the inner Jovian magnetosphere. It is contaminated with sulfur and oxygen ions due to the intense volcanic activity of one of Jupiter's moon Io, spewing plumes of sulfur dioxide ([Russell et al. 2001](#); [Bagenal 2007](#)).

Plasmas support multiple types of waves and instabilities, and the resonant wave-particle interaction is possible in several frequency domains. Waves in the ion cyclotron

† Email address for correspondence: yevgen.kazakov@rma.ac.be

(IC) range of frequencies are particularly sensitive to the presence of various ion species in the plasma. Resonant wave events in the IC frequency range are known to be strongly dependent on the plasma ion composition. Furthermore, the presence of multiple ion species, even with small concentrations, can lead to the appearance of new and modified resonance, cutoff, and crossover frequencies (André 1985). The origin of the waves can be different, and various types of polarization (primarily left-hand, right-hand, and linearly polarized waves) have been reported in the literature (e.g. Young et al. (1981); Boardsen (2012)).

Particle instruments have difficulties measuring the properties of the cold plasma because of spacecraft charging effects and also simply because the flux of low velocity particles is low. As mentioned in Denton et al. (2011), despite many years of magnetospheric research, there exists little precise knowledge of the bulk plasma composition within the inner magnetosphere. This is not only due to measurement difficulties but also, because the plasma composition is changing in space and time. Denton et al. (2011) reported major changes in the bulk plasma composition at geosynchronous orbit with respect to the solar cycle. Also, Craven et al. (1997) highlighted, that the big spread in the data on He^+/H^+ density ratio reflects its significant dependence on the latitude and local magnetic time.

Already in one of the first papers on wave propagation in multi-ion component plasmas, Smith and Brice (1964) noted that the ion-ion hybrid (IIH) resonance and cutoff frequencies present in plasmas with two or more ion species carry the information on ion densities. This motivated the development of indirect methods to determine the plasma composition using wave polarization analysis. Such an approach was used by Stasiewicz et al. (1994), who inferred the plasma composition using the lower hybrid and the IIH frequencies observed by the Freja satellite. They estimated the concentrations of H^+ , He^+ and O^+ ions to be 23%, 19% and 58%, respectively, at an altitude of 1700 km above the Earth. Later, Takahashi et al. (2008) analyzed ion composition in the plasma trough and plasma plume for the CRRES spacecraft orbit 962. They reported significant concentrations of oxygen ions in the low density region of plasma trough ($L \simeq 3.8 - 5.7$): O^+ ions were found to carry $\sim 50\%$ of the number density and $\sim 90\%$ of the mass density. However, oxygen was shown to be much less abundant in the plasma plume ($L \geq 6$).

Polarization analysis was recently applied by Sakaguchi et al. (2013) to compute the ion composition in the deep inner magnetosphere using the Akebono satellite measurements. Negligible oxygen content was reported and the ion composition ($\text{H}^+, \text{He}^+, \text{O}^+$) = (83%, 16%, 1%) was retrieved from the measured wave spectrogram. Relying on GOES-8 and GOES-10 data, somewhat lower helium concentrations ($X[\text{He}^+] = 6 - 16\%$) were inferred by Fraser et al. (2005a) for the plasma near the geostationary orbit. According to Fraser et al. (2005b), ion composition measurements identified He^+ as the second most abundant ion in the plasmasphere after protons. However, the oxygen content was observed to enrich during substorms and just inside the plasmopause (“oxygen torus”), where its density was found to increase by a factor of 10 whereas there is no corresponding variation in helium and proton concentrations.

Analysis of the wave polarization can give insight into the physical characteristics of waves and help understand their propagation and excitation mechanisms. In this paper, we focus on studying a particular type of the ultra-low-frequency (ULF) waves that are linearly polarized within a narrow frequency band with a resonant frequency below the local proton gyrofrequency, but larger than the gyrofrequency of heavy ions. Such IC waves have been detected in the magnetospheres of Earth and of Mercury (Young et al. 1981; Perraut et al. 1984; Russell 1989; Boardsen 2012). There is an ongoing discussion on the origin of these resonant waves. First, Russell (1989) argued that the observed

ULF wave was a standing Alfvén wave along the magnetic field line. Then, [Othmer et al. \(1999\)](#) developed a model for the field line resonances in Mercury’s magnetosphere accounting for multi-ion plasma composition and suggested the crossover frequency to be the preferred resonant frequency. Whereas for parallel propagation linear polarization occurs at the crossover frequency, fast magnetosonic (compressional) waves propagating across the magnetic field lines are polarized linearly at the IIIH resonant frequency. Alternatively, [Kim et al. \(2008\)](#) performed wave simulations in electron-proton-sodium plasmas and concluded that linearly polarized IC waves can be generated due to mode conversion (MC), which the fast wave undergoes at the the IIIH and/or Alfvén resonances. The additional IIIH resonance appears in plasmas, which include at least two ion species with the different charge-to-mass ratios, and gets its name because the resonant frequency occurs between the two IC frequencies. Further numerical studies by [Kim et al. \(2011\)](#) revealed that wave absorption is much more efficient at the IIIH resonance than at the Alfvén resonance. In our recent papers ([Kazakov & Fülöp 2013](#); [Fülöp & Kazakov 2014](#)), we complemented previous approaches and proved that efficient tunneling and mode conversion requires the resonant IIIH frequency to be close to the crossover frequency (but somewhat below) for typical conditions of the magnetospheres of Earth and Mercury. This means that the above mentioned explanations are not contradictory to each other.

Since the resonant IIIH frequency is linked to the plasma composition, solving the inverse problem allows one to infer the concentration of the heavy ions from the measured frequency spectra. In this paper, we identify numerically the conditions, when the MC efficiency is maximized in the magnetospheric plasmas of Earth and Mercury, and confirm analytical results derived in [Kazakov & Fülöp \(2013\)](#). Whereas for Mercury’s plasma, the resonant IIIH frequency is computed to be ≥ 0.8 of the crossover frequency, for the magnetospheric plasmas close to the geostationary orbit the IIIH frequency is proved to be very close to the crossover frequency. Due to arguments given above, we will start our analysis considering two-ion proton-helium plasma at this region and introduce later the effect of plasma contamination with oxygen ions. This potentially allows to estimate the helium concentration from the recorded ULF spectrogram relying on the two-ion plasma approximation or to provide an equation linking He^+ and O^+ concentrations if the oxygen content can not be neglected.

The rest of the paper is organized as follows. In section 2 we discuss the conditions when MC is efficient in magnetospheric plasmas. In section 3 we supplement previous analytical analysis with numerical MC computations and determine quantitatively how close the resonant IIIH frequency is to the crossover frequency for the typical parameters of Earth’s and Mercury’s plasmas. In section 4 we analyze the properties of the waves close to the crossover condition and evaluate the range of the parallel wave numbers yielding efficient MC. Finally, in section 5 we evaluate the frequency width of the spectrum for Mercury’s plasma and compare it to the experimentally reported value in [Russell \(1989\)](#). We conclude our results in section 6.

2. Conditions for efficient mode conversion

Propagation of fast magnetosonic waves (FW) through the inhomogeneous magnetosphere is treated by using a 1D slab plasma model ([Kim et al. 2008, 2011](#); [Kazakov & Fülöp 2013](#)). In spite of its simplicity, such a model captures the main features of the resonant MC process. We consider the incoming FW to be launched at the outer magnetosphere side and study its penetration to the inner regions of the magnetosphere. The dispersion relation for FW propagating predominantly across the

magnetic field lines is approximately given by (Stix 1992)

$$n_{\perp,\text{FW}}^2 = \frac{(\epsilon_{\text{L}} - n_{\parallel}^2)(\epsilon_{\text{R}} - n_{\parallel}^2)}{\epsilon_{\text{S}} - n_{\parallel}^2}, \quad (2.1)$$

where $n_{\parallel} = ck_{\parallel}/\omega$ is the parallel (along the magnetic field) refractive index, and $f = \omega/2\pi$ is the wave frequency. In Eq. (2.1), $\epsilon_{\text{S}} = \epsilon_1$, $\epsilon_{\text{L}} = \epsilon_1 - \epsilon_2$ and $\epsilon_{\text{R}} = \epsilon_1 + \epsilon_2$ are the plasma dielectric tensor components in the notation of Stix. In the cold-plasma limit and for the IC frequency range the tensor components can be written as

$$\epsilon_1 \simeq - \sum_i \frac{\omega_{pi}^2}{\omega^2 - \omega_{ci}^2}, \quad \epsilon_2 \simeq - \sum_i \frac{\omega}{\omega_{ci}} \frac{\omega_{pi}^2}{\omega^2 - \omega_{ci}^2}, \quad \epsilon_{\text{L,R}} \simeq \sum_i \frac{\omega_{pi}^2}{\omega_{ci}(\omega_{ci} \mp \omega)}, \quad (2.2)$$

where the summation is to be taken over all ion species constituting the plasma (protons and heavy ions), and ω_{pi} and ω_{ci} are the plasma and cyclotron frequencies of ions, respectively. The vacuum and electron contributions to ϵ_1 have been neglected because of their smallness with respect to the ion terms. Non-negligible electron contribution to ϵ_2 has already been included using the quasi-neutrality identity $\sum_i \omega_{pi}^2/\omega_{ci} = \omega_{pe}^2/|\omega_{ce}|$.

Figure 1 shows the radial dependence of $n_{\perp,\text{FW}}^2$ (Eq. (2.1)) computed for the plasma conditions near the geostationary orbit. The magnetospheric magnetic field is intrinsically inhomogeneous and is assumed to vary as $B(R) = B_E(R_E/R)^3$, where $B_E = 31 \mu\text{T}$ is the magnetic field at magnetic equator of the Earth. The plots are computed for the wave frequency $f = 0.72 \text{ Hz}$ and plasma density $n_e = 10 \text{ cm}^{-3}$, and assuming plasma to be composed of protons and helium ions with $X[\text{He}^+] = n_{\text{He}^+}/n_e = 39.4\%$. Whereas Fig. 1(a) stands for the special case of strictly perpendicular propagation ($k_{\parallel} = 0$), Fig. 1(b) is plotted accounting for a finite $k_{\parallel} = 5 \times 10^{-6} \text{ m}^{-1}$. The radial variation of n_{\perp}^2 depicted in Fig. 1 is typical for plasmas composed of two ion species: one can clearly see that there is a radial region where $n_{\perp}^2 \rightarrow \infty$. It occurs when the wave frequency matches locally the ion-ion hybrid frequency, which is defined by the condition

$$\epsilon_{\text{S}} = n_{\parallel}^2. \quad (2.3)$$

The IHH resonance does not appear in single-ion species plasmas and arises if at least two ion species with different charge-to-mass ratios are present in a plasma. The resonant IHH frequency satisfies $\omega_{c2} < \omega_{\text{S}} < \omega_{\text{cH}}$ (subindex ‘2’ refers to heavy ions). At the IHH resonant layer $R = R_{\text{S}}$, the incoming FW is partially converted to a shorter wavelength mode (slow/shear Alfvén wave or ion Bernstein wave). Within the adopted model, this appears as the resonant FW absorption. However, due to the radial inhomogeneity of the magnetic field the IHH resonance layer is accompanied by the L-cutoff layer $R = R_{\text{L}}$ to the lower magnetic field side, which is determined by the condition $\epsilon_{\text{L}} = n_{\parallel}^2$. Before reaching the resonance, the incoming FW first meets the cutoff layer and is partially reflected there. The IHH resonance and L-cutoff layers form together the MC layer ($R_{\text{S}} \leq R \leq R_{\text{L}}$), which is a barrier for the propagating FW since within this region the FW is evanescent, i.e. $n_{\perp,\text{FW}}^2 < 0$. The FW power transmits its power through the MC layer via tunneling. Only a fraction $\mathcal{T} = e^{-\pi\eta}$ of the incoming power tunnels through the layer, where η is the tunneling factor, roughly being a product of the asymptotic FW perpendicular wave number and the MC layer width. More rigorously, it has been defined as (Swanson 1998; Kazakov et al. 2010)

$$\eta = \frac{2}{\pi} \int_{R_{\text{S}}}^{R_{\text{L}}} |k_{\perp,\text{FW}}(R)| dR, \quad (2.4)$$

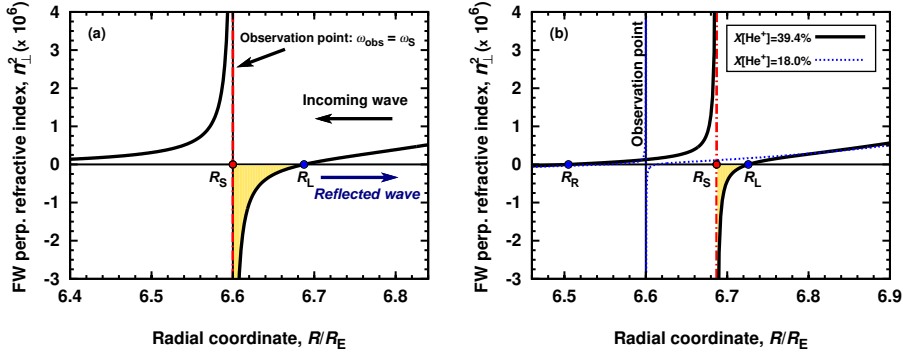


FIGURE 1. Radial dependence of the FW dispersion $n_{\perp, \text{FW}}^2$: $f = 0.72$ Hz, $B(R) = B_0(R_E/R)^3$, $n_e = 10 \text{ cm}^{-3}$: (a) $k_{\parallel} = 0$ and $X[\text{He}^+] = 39.4\%$; (b) $k_{\parallel} = 5 \times 10^{-6} \text{ m}^{-1}$ and $X[\text{He}^+] = 39.4\%/18.0\%$ (solid/dotted line). Mode conversion layer is depicted as the shaded area.

where $k_{\perp, \text{FW}} = (\omega/c)n_{\perp, \text{FW}}$ is the FW perpendicular wave number, which is an imaginary number within the MC layer.

In case of low k_{\parallel} and the isolated MC layer (Fig. 1(a)), the reflection coefficient for the waves excited at the outer magnetosphere (coming from the L-cutoff side) is given by $\mathcal{R} = (1 - \mathcal{T})^2$, limiting the conversion efficiency to be (Budden 1985)

$$\mathcal{C}^{(\text{Budden})} = \mathcal{T}(1 - \mathcal{T}). \quad (2.5)$$

If the transmitted FW undergoes additional wave reflection, once a right-hand polarized R-cutoff ($\epsilon_R = n_{\parallel}^2$) or a supplementary MC layer is present in a plasma, the resulting reflection and mode conversion coefficients depend on the constructive/destructive interference between the partially reflected fast waves (Majeski et al. 1994; Fuchs et al. 1995; Ram et al. 1996; Kazakov et al. 2010; Kim et al. 2011). For the cutoff-resonance-cutoff triplet (see Fig. 1(b)), an accurate analytical expression for the conversion efficiency was derived by Fuchs et al. (1995) and Ram et al. (1996). It is given by

$$\mathcal{C}^{(\text{triplet})} = 4\mathcal{T}(1 - \mathcal{T}) \sin^2(\Delta\phi/2). \quad (2.6)$$

Whereas for the isolated MC layer, the maximum MC efficiency is only 25%, for the triplet configuration it may be enhanced up to 100%. The enhanced MC efficiency requires the following two conditions to be satisfied simultaneously: (i) the phase difference is $\Delta\phi = (2n + 1)\pi$, $n \in \mathbb{Z}$ (the reflected waves have opposite phases and tend to cancel each other, thereby minimizing the resultant reflected wave); (ii) the MC layer is semi-transparent $\eta = \ln 2/\pi \approx 0.22$ ($\mathcal{T} = 1/2$). The latter condition for maximizing MC efficiency is common for the Budden and triplet models, and our analysis focuses on identifying proper conditions for that.

Kazakov & Fülöp (2013) derived an analytical expression for the tunneling factor for FW with $k_{\parallel} \simeq 0$ as a function of the heavy ion concentration. If the heavy ion concentration is not too small, the tunneling factor for plasmas of the terrestrial and the Hermian magnetospheres was proven to be $\eta \gg 1$. Provided the MC layer is non-transparent ($\eta \gg 1$), both Budden and triplet models predict that the incoming wave is almost totally reflected at L-cutoff and can not tunnel via the barrier and undergo mode conversion. E.g., for $\eta = 2$, $\mathcal{C}^{(\text{Budden})} \approx 0.2\%$, whereas $\mathcal{C}_{\text{max}}^{(\text{triplet})} = 4\mathcal{T}(1 - \mathcal{T}) \approx 0.8\%$. On the contrary, it was shown that MC can be efficient for waves with $k_{\parallel}/k_{\parallel}^* \lesssim 1$, where k_{\parallel}^*

is the FW critical parallel wave number defined as

$$k_{\parallel}^* = \frac{\omega_{\text{pH}}}{c} \frac{(f/f_{\text{cH}})}{\sqrt{\mathcal{Z}_1 + \mathcal{Z}_2}}. \quad (2.7)$$

Here, $\omega_{\text{pH}} = \sqrt{4\pi n_e e^2/m_{\text{H}}}$ is a reference proton plasma frequency, $\mathcal{Z}_1 = Z_1/A_1 = 1$ and $\mathcal{Z}_2 = Z_2/A_2$ are the ratios of the charge number to the atomic mass for protons and heavy ions, respectively, and f/f_{cH} is the ratio of the measured resonant ULF frequency to the local gyrofrequency of protons. Note that k_{\parallel}^* depends on the plasma density and scales linearly with the wave frequency and is independent of the heavy ion concentration and the radius of the planet. When k_{\parallel} is close to the critical k_{\parallel}^* , the FW dispersion includes R-cutoff (Kim and Johnson 2014) and evaluation of η from Eq. (2.4) allows to estimate the tunneling of the incoming FW and determine whether MC can be efficient (Kazakov & Fülöp 2014).

3. Inferring heavy ion concentration

Typically, the concentration of heavy ions in magnetospheric plasmas is not known *a priori*. Here, we describe briefly how this can be estimated from the recorded resonant ULF spectrogram if the assumption of two-ion species plasma is justified. As follows from Eqs. (2.2) and (2.3), the position of the IHH resonance in a plasma depends mainly on three quantities: wave frequency, heavy ion concentration and FW parallel wave number. For the measured wave frequency $f = f_{\text{obs}}$, a set of (k_{\parallel}, X_2) -values satisfies the FW resonant condition $\epsilon_1 = n_{\parallel}^2$ at the given observation point (cf. Figs. 1(a) and (b) computed for different $X[\text{He}^+]$)

$$\begin{aligned} X_2 &= X_{\min} + (X_{\max} - X_{\min})(1 - (k_{\parallel}/k_{\parallel}^*)^2), \\ X_{\min} &= \frac{(f/f_{\text{cH}})^2 - \mathcal{Z}_2^2}{\mathcal{Z}_1^2 - \mathcal{Z}_2^2}, \quad X_{\max} = \frac{\mu X_{\min}}{1 + (\mu - 1)X_{\min}}, \end{aligned} \quad (3.1)$$

where $X_2 = Z_2 n_2/n_e$ is the *unknown* concentration of heavy ions multiplied by their charge number, and $\mu = \mathcal{Z}_1/\mathcal{Z}_2$. As an *input* value for inferring the heavy ion concentration, we use the ratio of the resonant ULF frequency to the local gyrofrequency of protons f/f_{cH} . If one calculates the exact value of k_{\parallel} yielding the maximized MC, the corresponding heavy ion concentration can be determined from Eq. (3.1). Its value is between X_{\min} and X_{\max} , both of which, in turn, depend on f/f_{cH} .

As an example, we consider two linearly polarized ULF wave events, at Mercury's magnetosphere (including a significant fraction of heavy sodium ions Na^+) detected by the Mariner 10 spacecraft and at the Earth's magnetosphere (including helium ions) detected by the GEOS satellite. In the case of Mercury, the spectral intensity was peaked at frequency $f \approx 0.5$ Hz (Russell 1989). The local magnetic field strength was $B \approx 86$ nT and hence proton and sodium gyrofrequencies were $f_{\text{cH}} \approx 1.31$ Hz and $f_{\text{c,Na}^+} \approx 0.057$ Hz. In the case of Earth, the observed frequency was $f \approx 1.0$ Hz, whereas the local proton gyrofrequency was $f_{\text{cH}} \approx 2.28$ Hz (Perraut et al. 1984).

Figure 2(a) shows the (k_{\parallel}, X_2) -diagram computed for the conditions of Earth's ($R = 6.6R_{\text{E}}$ and $n_e = 10 \text{ cm}^{-3}$) and Mercury's ($R = 1.5R_{\text{M}}$ and $n_e = 3 \text{ cm}^{-3}$) magnetospheres, choosing the input frequency ratios $f/f_{\text{cH}} \approx 0.44$ and 0.38, respectively. For the chosen f/f_{cH} and for any individual k_{\parallel} , the dispersion relation (2.1) is evaluated numerically for different X_2 finding the proper one (shown with circles), for which the IHH resonance is located at the considered radial position. The solid lines show the heavy ion concentration as predicted by Eq. (3.1). It is clear that there is excellent agreement

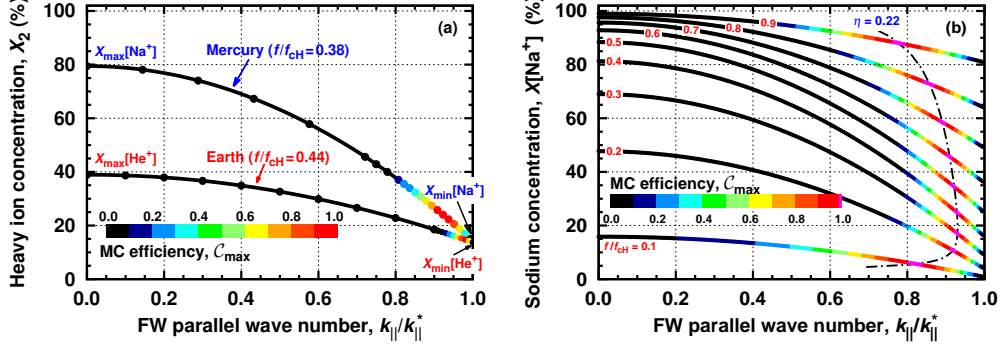


FIGURE 2. (a) Heavy ion concentration vs. the FW parallel wave number for the fixed IHH resonance location. The colour of the points represents the maximum MC efficiency, $C_{\max} = 4\mathcal{T}(1 - \mathcal{T})$. (b) The $(k_{\parallel}, X[\text{Na}^+])$ -diagram for the different f/f_{cH} ratios for Mercury's plasma. The dash-dotted line shows $\eta = 0.22$ and maximized MC efficiency ($C_{\max} = 100\%$).

between the numerical results and Eq. (3.1), and the algebra behind this equation is correct. In addition, for every pair of (k_{\parallel}, X_2) values we evaluated numerically the tunneling factor using Eq. (2.4) and the maximum MC efficiency $C_{\max} = 4\mathcal{T}(1 - \mathcal{T})$. The latter is represented by the colour of the circles.

Taking the Mercury case as an example, one can consider two different extreme cases for the measured $f/f_{cH} \approx 0.38$. If the detection of waves with $k_{\parallel} \simeq 0$ is assumed, then the IHH resonant frequency ω_S reduces to the well-known Buchsbaum two-ion hybrid frequency

$$\omega_{S0} = \omega_{c2} \sqrt{\frac{1 - (1 - \mu)X_2}{1 - (1 - 1/\mu)X_2}},$$

which satisfies $\epsilon_1(\omega_{S0}) = 0$. However, for such k_{\parallel} and for the considered plasma conditions of Earth and Mercury, $\eta \gg 1$ and the MC layer is non-transparent, and therefore the FW cannot tunnel through the barrier and undergo mode conversion (Kazakov & Fülöp 2013). The other limiting case corresponds to $k_{\parallel} = k_{\parallel}^*$ and $X_2 = X_{\min}$. For these parameters, the IHH resonance, L-cutoff and R-cutoff intersect at the observation point such that the MC layer width and accordingly also the tunneling factor reduce to zero. This occurs for $\epsilon_2(\omega_{\text{cross}}) = 0$ (ϵ_2 is a non-diagonal tensor element), and is typically referred to as the crossover condition (Othmer et al. 1999). The crossover frequency in a two-ion species plasmas is linked to the heavy ion concentration as

$$\omega_{\text{cross}} = \omega_{c2} \sqrt{1 + (\mu^2 - 1)X_2}.$$

According to Fig. 2(a), for the measured frequency ratio for Mercury's plasma ($f/f_{cH} \approx 0.38$), the sodium concentration is between $X_{\min}[\text{Na}^+] = 14.3\%$ and $X_{\max}[\text{Na}^+] = 79.3\%$. For the frequency ratio $f/f_{cH} \approx 0.44$ reported for Earth by Perraut et al. (1984), Eq. (3.1) implies that the helium concentration is between $X_{\min}[\text{He}^+] = 14.0\%$ and $X_{\max}[\text{He}^+] = 39.4\%$. These values, which correspond to the Buchsbaum ($k_{\parallel} = 0$, $\eta \gg 1$) and the crossover ($k_{\parallel} = k_{\parallel}^*$, $\eta = 0$) conditions, yield the *upper* and the *lower* estimates for the heavy ion concentration, respectively.

Since efficient MC requires $0.05 \leq \eta \leq 0.61$ (these are the tunneling factors at which $C_{\max} = 50\%$) and is maximized at $\eta \approx 0.22$ (Kazakov & Fülöp 2013), one can conclude that the FW parallel wave number should be close to, but somewhat below, k_{\parallel}^* . This is also illustrated in Fig. 2(b), which shows the (k_{\parallel}, X_2) -diagram for various f/f_{cH} in the

case of Mercury. The dash-dotted line in Fig. 2(b) depicts the optimal case $\eta = 0.22$, which leads to the maximized MC efficiency ($\mathcal{C}_{\max} = 100\%$) and determines the sodium concentration as a function of the observed frequency.

For $X_2 = X_{\min}$, decreasing k_{\parallel} will result in a non-zero MC layer width. Simultaneously, the resonant layer will be shifted to the higher magnetic field side relative to the observation point. As a result, the heavy ion concentration should be somewhat larger than X_{\min} to displace the resonant layer in the opposite direction and locate it back at the observation point (for the fixed wave frequency). This opposite shift of the IIIH resonant layer due to the change of k_{\parallel} and X_2 is captured by Eq. (3.1): for any heavy ion concentration within the range $X_{\min} \leq X_2 \leq X_{\max}$, there exists a particular wave number k_{\parallel} , for which the IIIH resonance is located at the point of observation.

As follows from Fig. 2(a), the maximum MC efficiency ($\mathcal{C}_{\max} = 1$) is reached at $k_{\parallel}/k_{\parallel}^* \approx 0.93$ and 0.98 for the plasmas of Mercury and Earth, respectively. Once this wave number ratio is known, the heavy ion concentration can be easily evaluated. For Earth, Eq. (3.1) yields $X[\text{He}^+] \approx 15.1\%$, while for Mercury $X[\text{Na}^+] \approx 23.3\%$. The computed value for the sodium concentration – as expected – is somewhat larger than $X[\text{Na}^+] \approx 14\%$ reported by Othmer et al. (1999), who analyzed the same wave event and used the crossover frequency itself as a preferred resonant ULF frequency. Note that the values we obtain for $X[\text{Na}^+]$ are in very good agreement with the results of more sophisticated numerical modeling performed by Kim et al. (2011), who accounted for the additional FW reflection at R-cutoff and wave interference (shown with open circles in Fig. 3(a)). For $\omega_S/\omega_{\text{cH}} = 0.4$, a sodium concentration $X[\text{Na}^+] = 25\%$ was reported. This is not surprising since – as already mentioned – efficient mode conversion requires the evanescence layer to be a semi-transparent ($\mathcal{T} \simeq 1/2$), regardless if the Budden or the triplet MC model is used. Figure 2(b) is also consistent with another two cases considered by Kim et al. (2011), viz. $(\omega_S/\omega_{\text{cH}}; X[\text{Na}^+]) = (0.2; 12\%)$ and $(0.6; 45\%)$.

The ratio of the IIIH resonant to the crossover frequency is also linked to the $k_{\parallel}/k_{\parallel}^*$ value

$$p = \omega_S/\omega_{\text{cross}} = \left[1 + G(x) \left(1 - (k_{\parallel}/k_{\parallel}^*)^2 \right) \right]^{-1/2}, \quad (3.2)$$

$$G(x) = \frac{(x^2 - \mathcal{Z}_2^2)(\mathcal{Z}_1^2 - x^2)}{x^2(\mathcal{Z}_1\mathcal{Z}_2 + x^2)},$$

where we introduced $x = f/f_{\text{cH}}$. Equation (3.2) predicts $p \approx 0.97$ for the plasma conditions of the terrestrial magnetosphere near the geostationary orbit, whereas for Mercury's plasma $p \approx 0.79$, in agreement with the values reported by Kazakov & Fülöp (2014). Vice versa, if the $\omega_S/\omega_{\text{cross}}$ ratio is known, by combining Eqs. (3.1) and (3.2), the next-order correction to the heavy ion concentration can be determined to be

$$X_2/X_{\min} = (x^2/p^2 - \mathcal{Z}_2^2)/(x^2 - \mathcal{Z}_2^2) \gtrsim 1. \quad (3.3)$$

For Mercury, this can be simplified further since $\mathcal{Z}_2 = 1/23 \ll 1$, and $X[\text{Na}^+] \approx X_{\min}[\text{Na}^+]/p^2$.

As provided by our simplified MC analysis, Figure 3 illustrates the estimates of the sodium and helium concentrations as functions of resonant frequency in the magnetospheres of Mercury and Earth, respectively. With green dash-dotted and orange dash-double-dotted lines we show the minimum and maximum values of the heavy ion concentrations (Eq. (3.1)), and with red solid line we show the estimated heavy ion concentration determined from $\mathcal{C}_{\max} = 100\%$. In the same figure, the ratio $k_{\parallel}/k_{\parallel}^*$ and $\omega_S/\omega_{\text{cross}}$ is plotted with dashed and dotted line, respectively. Note that whereas for

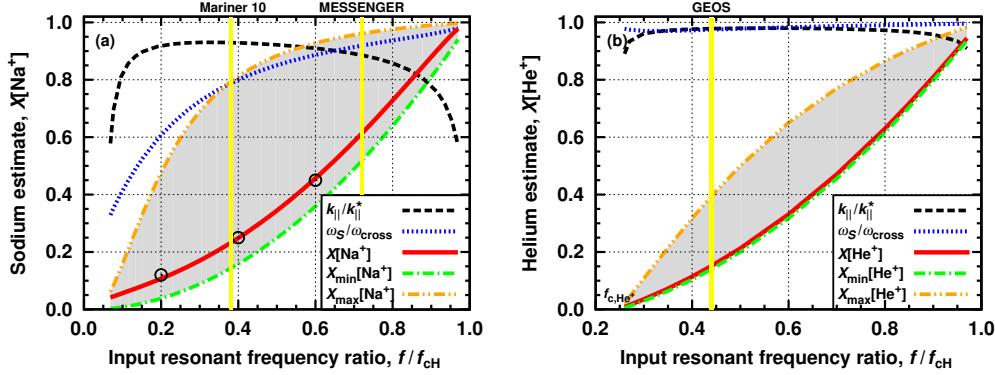


FIGURE 3. (a) and (b) Sodium and helium concentrations vs. the measured frequency ratio f/f_{cH} for the magnetospheres of Mercury and Earth, respectively. Open circles in Fig. 3(a) correspond to the data reported by Kim et al. (2011).

Mercury’s plasma the resonant frequency ω_S is close to the crossover frequency (according to Fig. 3(a), $p \approx 0.8$ for Mariner 10 and $p \approx 0.9$ for MESSENGER observations, $f/f_{cH} \simeq 0.7$ reported by Boardson (2012)), for the magnetosphere of Earth the resonant IIIH frequency is even closer to the crossover frequency ($p \approx 0.97$) (see Fig. 3(b)).

The numerical results shown in Fig. 3 can be interpreted by using Eq. (3.2). As a function of f/f_{cH} , $G(x)$ in Eq. (3.2) maximizes at $\hat{x} = \mathcal{Z}_1 / \sqrt{\mu^{3/2} - \mu + \mu^{1/2}}$ and equals to $\hat{G} = (1 + 1/\mu)(\sqrt{\mu} - 1)^2$. This yields for Earth $\hat{G}_{\text{Earth}} = 1.25$ but it is substantially larger for Mercury $\hat{G}_{\text{Mercury}} \approx 15.0$. For the measured f/f_{cH} values, the magnitude of the G -term and the difference in the computed $k_{\parallel}/k_{\parallel}^*$ values, contribute equally to the fact why the $\omega_S/\omega_{\text{cross}}$ ratio is much closer to one for Earth than for Mercury ($G_{\text{Earth}}(0.44) \approx 1.2$ vs. $G_{\text{Mercury}}(0.38) \approx 4.5$).

The fact that for plasmas near the geostationary orbit, the resonant IIIH frequency is very close to the crossover frequency, potentially allows an accurate determination of $X[\text{He}^+]$ by matching f_{obs} to f_{cross} , without a need to go to the second-order approximation as in case of Mercury. However, this holds only if the two-ion species approximation is justified. Otherwise, one needs to account for the upshift/downshift of the crossover frequency due to the presence of additional ion species, e.g. O^+ . This effect is more important for the Earth’s magnetosphere than the correction due to the finite p -value. Following the reasoning presented in Kazakov & Fülöp (2013), one can show that the heavy ion concentration satisfying the crossover condition, in general case, is given by

$$\sum_{i=2,3,\dots} \frac{\mathcal{Z}_1^2 - \mathcal{Z}_i^2}{(f/f_{cH})^2 - \mathcal{Z}_i^2} X_i = 1, \quad (3.4)$$

where the sum is over all ion species, except of the majority proton ions. Similar analysis was given by Othmer et al. (1999) to correct the sodium estimate accounting for additional contamination of Hermean plasma with He^{2+} ions. If we use the same frequency ratio $f/f_{\text{obs}} = 0.38$ reported by Russell (1989), Eq. (3.4) predicts $X[\text{Na}^+] \approx 0.143 + 2.03n_{\text{He}^{2+}}/n_e$ (note that in our notations $X[\text{He}^{2+}] = 2n_{\text{He}^{2+}}/n_e$). Hence, Eq. (3.4) is the generalization of Eq. (33) by Othmer et al. (1999). Note that Eq. (3.4) is not restricted for plasmas with three ion species but is correct for an arbitrary number of ion species. However, a complete determination of the plasma composition is not possible in this case (the number of unknowns exceeds the number of equations) without

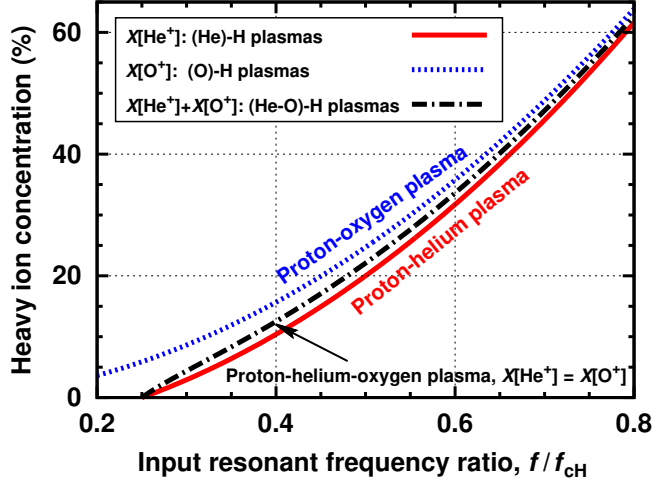


FIGURE 4. Heavy ion concentrations satisfying the crossover frequency in proton-helium-oxygen plasmas.

having information on the concentrations of additional ion species or setting up another constraints. For example, for Mercury’s plasma Othmer et al. (1999) assumed a mixing ratio for Na^+ and He^{2+} constituents to be the same as in the the solar wind, and that provided the additional constraint necessary for determining the plasma composition.

Figure 4 shows the heavy ion concentrations satisfying the crossover frequency in proton-helium-oxygen plasmas. The red solid curve for the proton-helium plasma is exactly the same as the curve showing $X_{\min}[\text{He}^+]$ in Fig. 3(b). The blue dotted line depicts another limiting case of the proton-oxygen plasma. For the same resonant frequency ratio, the estimated oxygen concentration is somewhat higher than that of helium, in line with Eq. (3.1). For $f/f_{cH} = 0.44$, Eq. (3.4) predicts $X[\text{He}^+] + 0.73X[\text{O}^+] \approx 0.14$, and one gets $X[\text{He}^+] = 14\%$ for (He)-H plasmas and $X[\text{O}^+] = 19\%$ for (O)-H plasmas. Figure 4 also displays the intermediate case, when the helium and oxygen concentrations are assumed to be equal (dashed-dotted line). For the given resonant ULF frequency, $X[\text{He}^+] + X[\text{O}^+] \approx 16\%$. This example shows that the presented approach still provides reasonably fair estimate for the total heavy ion concentration, even if one has no a priori information on the helium/oxygen density ratio.

4. Tunneling factor at the crossover condition

By applying the least-square fitting of the numerical results for η computed using Eq. (2.4), we find that the tunneling factor for $k_{\parallel}/k_{\parallel}^* \lesssim 1$ scales as (see Fig. 5(a))

$$\eta(k_{\parallel}) \approx a_{\text{fit}} \left(1 - k_{\parallel}/k_{\parallel}^*\right)^{3/2}. \quad (4.1)$$

For the considered conditions of magnetospheric plasmas, $a_{\text{fit}} \approx 12$ for Mercury and $a_{\text{fit}} \approx 65$ for Earth (assuming (He)-H plasma), respectively. Then, using Eq. (4.1), the FW parallel wave number, at which $\eta = 0.22$ and maximized MC occurs, can be derived

$$k_{\parallel}^{\dagger}/k_{\parallel}^* = 1 - 0.365a_{\text{fit}}^{-2/3}. \quad (4.2)$$

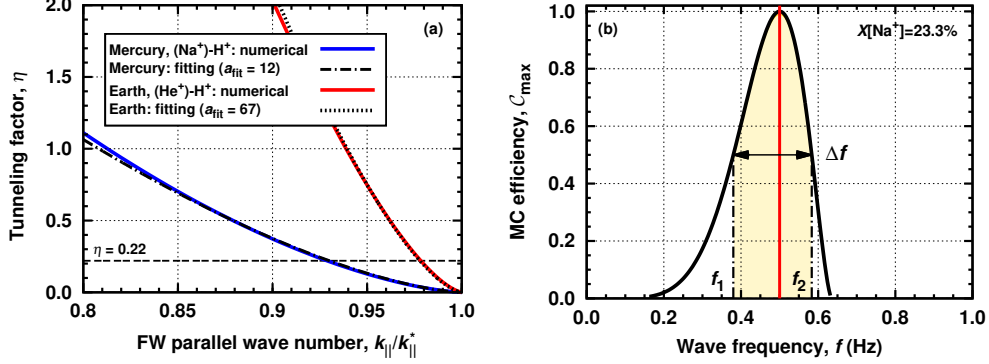


FIGURE 5. (a) Tunneling factor vs. k_{\parallel} at the crossover condition. (b) Computed MC efficiency C_{max} vs. the wave frequency for Mercury's plasma and $X[\text{Na}^+] = 23.3\%$.

If we use the computed numerical values for a_{fit} , $k_{\parallel}^{\dagger}/k_{\parallel}^* \approx 0.93$ and 0.98 are obtained, consistent with previous results. This approach also allows to estimate the range of k_{\parallel} , under which an efficient MC occurs ($0.05 \leq \eta \leq 0.61$, i.e. $C_{\text{max}} \geq 50\%$) once only a single value of k_{\parallel}^{\dagger} is known

$$\Delta k_{\parallel}/k_{\parallel}^* \approx 1.6(1 - k_{\parallel}^{\dagger}/k_{\parallel}^*). \quad (4.3)$$

The coefficient, which appears in the right-hand side of Eq. (4.3), reflects the power exponent identified in the scaling, viz. $1.6 \approx (0.61^{2/3} - 0.05^{2/3}) / (0.22^{2/3})$. This means that for Mercury's plasma the k_{\parallel} -spectrum where efficient MC occurs has a width $\Delta k_{\parallel}/k_{\parallel}^* \approx 0.11$, but for the Earth's plasma it is narrower, $\Delta k_{\parallel}/k_{\parallel}^* \approx 0.03$. Note that since our approach is based on evaluating C_{max} and neglecting the wave interference and the phase term in Eq. (2.6), the presented approximation for Δk_{\parallel} overestimates the actual value.

5. Frequency width of the wave spectrum

The measured wave spectrum has a finite frequency width Δf . For the ULF event in Mercury's magnetospheric plasma $\Delta f \approx 0.26 - 0.30$ Hz was reported by Russell (1989). Here, we investigate if that is consistent with our analysis and the assumption that the observed resonant ULF waves are due to mode conversion. To accomplish that, we apply a somewhat different reasoning: the sodium concentration is kept constant ($X[\text{Na}^+] \approx 23.3\%$), and the parallel wave number k_{\parallel} is adjusted for every frequency f according to Eq. (3.1), such that the IIH resonance is located at the point of observation. Figure 5(b) shows the computed C_{max} as a function of f . Again, the Buchsbaum ($k_{\parallel} = 0, \eta \gg 1$) and the crossover conditions ($k_{\parallel} = k_{\parallel}^*, \eta = 0$) can be clearly distinguished, represented by the two side frequencies at which $C_{\text{max}} \rightarrow 0$. In terms of the wave frequency these can be written as

$$f_{\text{min}} = f_{c2} \sqrt{\frac{1 - (1 - \mu)X_2}{1 - (1 - 1/\mu)X_2}} \approx 0.16 \text{ Hz}, \quad (5.1)$$

$$f_{\text{max}} = f_{c2} \sqrt{1 - (1 - \mu^2)X_2} \approx 0.635 \text{ Hz},$$

respectively. If we assume that the measured spectral intensity of the resonant linearly polarized ULF signal is proportional to the MC efficiency, then Δf requires the evaluation of the full width at half maximum for C_{max} : $C_{\text{max}} = 50\%$ is reached at $f_1 \approx 0.38$ Hz and $f_2 \approx 0.58$ Hz. Hence, for the considered conditions the spectrum is peaked at $\hat{f} = 0.5$ Hz

and has a frequency width $\Delta f = f_2 - f_1 \approx 0.20$ Hz. The computed value is in a qualitative agreement with the observations.

6. Conclusions

We have complemented previous analytical results derived in (Kazakov & Fülöp 2013) by evaluating the tunneling factor and the maximum MC efficiency \mathcal{C}_{\max} numerically for the magnetospheres of Earth and of Mercury. Efficient MC is shown to occur in a narrow range of k_{\parallel} close to the FW critical wave number k_{\parallel}^* , which depends mainly on the plasma density and the frequency f/f_{cH} ratio, and is independent of the radius of the planet and the heavy ion concentration. For the detected wave event in Mercury’s magnetosphere, ω_S is confirmed to be close, but somewhat below, the crossover frequency ($p \approx 0.8$ for Mariner 10 and $p \approx 0.9$ for MESSENGER observations). For the plasma conditions near the geostationary orbit, the resonant IIIH frequency is very close to the crossover frequency for a wide range of parameters ($p \approx 0.97$), potentially making an accurate estimate of the heavy ion concentration from some of the detected resonant linearly polarized ULF signals possible. For Mercury, the evaluated frequency width of the spectrum Δf has been shown to be consistent with the measured value.

Acknowledgements. The authors are grateful to the anonymous referees for the valuable improvements they suggested.

REFERENCES

- M. André, *J. Plasma Phys.* **33**, 1–19 (1985).
M. André and A. Yau, *Space Science Reviews* **80**, 27–48 (1997).
F. Bagenal, *J. Atmospheric and Solar-Terrestrial Phys.* **69**, 387–402 (2007).
S.A. Boardsen, J.A. Slavin, B.J. Anderson et al., *J. Geophys. Res.* **117**, A00M05 (2012).
K.G. Budden, *The Propagation of Radio Waves*, Cambridge University Press (1985).
A.F. Cheng, R.E. Johnson, S.M. Krimigis and L.J. Lanzerotti, *Icarus* **71**, 430–440 (1987).
P.D. Craven, D.L. Gallagher and R.H. Comfort, *J. Geophys. Res.* **102**, 2279–2289 (1997).
R.E. Denton, M.F. Thomsen, K. Takahashi, R.R. Anderson and H.J. Singer, *J. Geophys. Res.* **116**, A03212 (2011).
B.J. Fraser, H.J. Singer, M.L. Adrian, D.L. Gallagher and M.F. Thomsen, “The relationship between plasma density structure and EMIC waves at geosynchronous orbit”, in *Inner Magnetosphere Interactions: New Perspectives from Imaging* (eds J. Burch, M. Schulz and H. Spence), American Geophysical Union, Washington, D. C., 55–70 (2005a).
B.J. Fraser, J.L. Horwitz, J.A. Slavin, Z.C. Dent and I.R. Mann, *Geophys. Res. Lett.* **32** L04102 (2005b).
V. Fuchs, A.K. Ram, S.D. Schultz, A. Bers and C.N. Lashmore-Davies, *Phys. Plasmas* **2**, 1637–1647 (1995).
T. Fülöp and Ye.O. Kazakov, *Proc. 41st EPS Conf. on Plasma Physics* (23–27 June 2014, Berlin, Germany), P2.065 (2014).
W.-H. Ip, *Geophys. Res. Lett.* **13**, 423–426 (1986).
Ye.O. Kazakov, I.V. Pavlenko, D. Van Eester, B. Weyssow and I.O. Girka, *Plasma Phys. Control. Fusion* **52**, 115006 (2010).
Ye.O. Kazakov and T. Fülöp, *Phys. Rev. Lett.* **111**, 125002 (2013).
Ye.O. Kazakov and T. Fülöp, *Phys. Rev. Lett.* **113**, 089502 (2014).
E.-H. Kim, J.R. Johnson and D.-H. Lee, *J. Geophys. Res.* **113**, A11207 (2008).
E.-H. Kim, J.R. Johnson and K.-D. Lee, *Geophys. Res. Lett.* **38**, L16111 (2011).
E.-H. Kim and J.R. Johnson, *Phys. Rev. Lett.* **113**, 089501 (2014).
R. Majeski, C.K. Phillips and J.R. Wilson, *Phys. Rev. Lett.* **73**, 2204–2207 (1994).
C. Othmer, K.-H. Glassmeier and R. Cramm, *J. Geophys. Res.* **104**, 10369–10378 (1999).

- S. Perraut, R. Gendrin, A. Roux and C. de Villedary, *J. Geophys. Res.* **89**, 195–202 (1984).
- A.K. Ram, A. Bers, S.D. Schultz and V. Fuchs, *Phys. Plasmas* **3**, 1976–1982 (1996).
- C.T. Russell, *Geophys. Res. Lett.* **16**, 1253–1256 (1989).
- C.T. Russell, Y.L. Wang, X. Blanco-Cano and R.J. Stangeway, *J. Geophys. Res.* **106**, 26233–26242 (2001).
- K. Sakaguchi, Y. Kasahara, M. Shoji et al., *Geophys. Res. Lett.* **40**, 5587–5591 (2013).
- R.L. Smith and N. Brice, *J. Geophys. Res.* **69**, 5029–5040 (1964).
- K. Stasiewicz, G. Gustafsson, G. Holmgren et al., *Geophys. Res. Lett.* **21**, 1839–1842 (1994).
- T.H. Stix, *Waves in Plasmas*, AIP (1992).
- D.G. Swanson, *Theory of Mode Conversion and Tunneling in Inhomogeneous Plasmas*, Wiley (1998).
- K. Takahashi, S. Ohtani, R.E. Denton, W.J. Hughes and R.R. Anderson, *J. Geophys. Res.* **113**, A12203 (2008).
- A.W. Yau and M. André, *Space Science Reviews* **80**, 1–25 (1997).
- D.T. Young, S. Perraut, A. Roux et al., *J. Geophys. Res.* **86**, 6755–6772 (1981).
- T.H. Zurbuchen, J.M. Raines, J.A. Slavin et al., *Science* **333**, 1862–1865 (2011).